Mol Neurobiol (2016) 53:5679–5691
DOI 10.1007/s12035-015-9454-1

SMAD4 Defect Causes Auditory Neuropathy Via Specialized Disruption of Cochlear Ribbon Synapses in Mice

Ke Liu[1] · Fei Ji[1] · Guan Yang[2] · Zhaohui Hou[1] · Jianhe Sun[1] · Xiaoyu Wang[1] · Weiwei Guo[1] · Wei Sun[3] · Weiyan Yang[1] · Xiao Yang[2] · Shiming Yang[1]

Received: 3 June 2015 / Accepted: 25 September 2015 / Published online: 21 October 2015
© Springer Science+Business Media New York 2015

Abstract More than 100 genes have been associated with deafness. However, *SMAD4* is rarely considered a contributor to deafness in humans, except for its well-defined role in cell differentiation and regeneration. Here, we report that a *SMAD4* defect in mice can cause auditory neuropathy, which was defined as a mysterious hearing and speech perception disorder in human for which the genetic background remains unclear. Our study showed that a *SMAD4* defect induces failed formation of cochlear ribbon synapse during the earlier stage of auditory development in mice. Further investigation found that there are nearly normal morphology of outer hair cells (OHCs) and post-synapse spiral ganglion nerves (SGNs) in *SMAD4* conditional knockout mice (cKO); however, a preserved distortion product of otoacoustic emission (DPOAE) and cochlear microphonic (CM) still can be evoked in cKO mice. Moreover, a partial restoration of hearing detected by electric auditory brainstem response (eABR) has been obtained in the cKO mice using electrode stimuli toward auditory nerves. Additionally, the ribbon synapses in retina are not affected by this *SMAD4* defect. Thus, our findings suggest that this *SMAD4* defect causes auditory neuropathy via specialized disruption of cochlear ribbon synapses.

Keywords *SMAD4* · Deafness · Auditory neuropathy · Ribbon synapse · Cochlea · Retina

Introduction

Auditory neuropathy (AN) is a special type of sensorineural deafness which is characterized by abnormal or absent auditory brainstem responses (ABRs) in the presence of normal or preserved outer hair cell (OHC) function [1]. Among infants and children with permanent sensorineural deafness, the prevalence of AN is reported to range from 10 to 12 % [2]. Clinical features of AN include impairment of speech perception beyond what is expected for hearing loss. As of today, more than half of AN is estimated to be associated with genetic defects [3]. However, only a few causative genes have been identified as responsible for AN, including *OTOF*, *SLC17A8*, and *DIAPH3* [4–7]. *OTOF* encodes otoferlin (MIM 603681). Mutations in *OTOF* are responsible for DFNB9 (MIM 601071) deafness, which is characterized by absent ABRs with documentation of preserved OHC function in some patients [4, 8]. *SLC17A8*, which encodes the vesicular glutamate transporter-3 (VGLUT3), has been identified as the gene responsible for DFNA25 [6]. Although AN is not a rare form of hearing loss, the management of AN remains challenging for audiologists and speech therapists since identification of the underlying genetic causes and animal model comparisons have not been well developed. Without the understanding of an underlying mechanism, there has been generally poor outcomes in the management of AN. Therefore, to identify novel causative

Ke Liu and Fei Ji contributed equally to this work.

✉ Xiao Yang
yangx@bmi.ac.cn

✉ Shiming Yang
yangsm301@263.net

[1] Department of Otolaryngology, Head and Neck Surgery, The Institute of Otolaryngology, Chinese PLA General Hospital, 28 Fuxing Road, Beijing 100853, China

[2] The State Key Laboratory of Proteomics, Genetics Laboratory of Development and Disease, Institute of Biotechnology, AMMS, Beijing 100071, China

[3] Department of Communicative Disorders and Sciences, The State University of New York at Buffalo, Buffalo, NY 14214, USA

genes and construct animal models has become crucial to resolving the problem.

Our previous study found that *SMAD4* (mothers-against-DPP homolog 4; NM_005359) deficits may associate with sensorineural deafness in mice [9]. Our recent data revealed that there is an absence of ABR and a preserved distortion product of otoacoustic emission (DPOAE) response in mice with *SMAD4* defects, suggesting that *SMAD4* defects may associate with AN. Correspondingly, other studies have identified several mutations in *SMAD4* that are responsible for myhre syndrome (MIM139210), a rare developmental disorder characterized by short stature, short hands and feet, facial dysmorphism, muscular hypertrophy, and cognitive delay. In particular, deafness has been defined as one of the major features of this syndrome [10, 11].

The SMAD signaling pathway has been proposed to play an important role in bone morphogenetic protein (BMP) signaling. BMP, a member of the transforming growth factor β (TGF-β) superfamily, is crucial for cell differentiation and regeneration [12–16]. Although these findings revealed a correlation between *SMAD4* and deafness, no reliable evidence has been obtained so far to verify an underlying mechanism and whether *SMAD4* defects can specifically cause AN—a special type of deafness. Here, we report that the mice with conditional knockout of *SMAD4* display a potential animal model of auditory neuropathy (AN). Because there is no ABR response evoked in conditional knockout (cKO) mice, whereas, both preserved DPOAE and (CM) in cKO mice can be obtained. Further study showed that failed formation of cochlear ribbon synapse could be responsible for the hearing loss in the cKO mice. In this study, we have employed several experimental approach to achieve our goal confirming the animal model of AN with developmental problem of cochlear ribbon synapse which has been induced by *SMAD4* deficits.

Material and Methods

Generation of Mice with *SMAD4* Defect

In this study, the conditional *SMAD4* knockout mice were obtained as described previously [9, 17].

Auditory Functional Detection

Auditory Brainstem Response Analysis The hearing thresholds of the mice were determined by ABRs which have been tested in a soundproof room using the Smart EP system (Intelligent Hearing Systems, FL) in a double-blind paradigm. During the test, mice were anesthetized and their body temperature was maintained using a heating pad. Subdermal needle electrodes were inserted at the vertex and ventrolaterally to both ears for ABR tests. Both click and pure tone pips (4, 8, 16, and 32 kHz, 10–100 dB SPL, 5-dB step) were used for sound stimuli. The filter for ABR response was 100 to 3000 Hz. ABR thresholds were determined for each stimulus frequency by identifying the lowest intensity eliciting a reproducible ABR response.

Distortion Product Otoacoustic Emission Test DPOAE responses were recorded from anesthetized mice using the Smart DPOAE system. DPOAEs were elicited by two primary tones, F1 and F2, with an F2/F1 ratio of 1.2. L1 was set 10 dB higher than L2. F2 frequencies were set at 6 and 30 kHz for the mice. DPOAE input/output functions were obtained by decreasing the L2 intensity in 5-dB steps. Thirty-two sweeps were presented at each test level. These responses were then stored and displayed on a computer. The input/output functions of DPOAE were averaged for each tested frequency. The threshold of DPOAE was defined as 6 dB above the noise floor [18].

Compound Action Potential and Cochlear Microphonic Examination Compound action potential (CAP) and CM responses were recorded via a fine silver ball electrode on the round window. The cochlear response was amplified and filtered (100–3000 Hz) using Smart EP (Intelligent Hearing Systems, USA). Tone pips (5 ms duration) were used for CAPs and CM recordings.

Cochlear Tissue Preparation

SMAD4 conditional knockout mice ($SMAD4^{-/-}$) and *SMAD4* wild-type ($SMAD4^{+/+}$) littermates with documented dates of birth were obtained from the Chinese Academy of Medical Sciences (Beijing, China). No outer or middle ear pathology was encountered in any of the animals. All procedures were executed in accordance with an animal protocol approved by the Animal Care and Use Committee of the Institute of Biotechnology of AMMS and the Institute of Otolaryngology, the General Hospital of Chinese PLA. Mice were sacrificed by decapitation, and the temporal bones were removed and the cochleae were quickly separated. The round window, the oval window, and the apex of the cochlea were opened and then perfused with 4 % paraformaldehyde (PFA) in 10 mM phosphate buffered saline (PBS, pH 7.4) overnight at 4 °C. The cochlea shells were separated from the basal turn under a dissecting microscope in 0.01 mmol/L PBS solution. The parietal gyrus of the basilar membrane was then separated and the vestibular membrane and the covering membrane were removed.

Retinal Tissue Preparation

The preparation of retinal tissue for light and electron microscopy followed the protocol described by Dick et al. [19]. Briefly, for light microscopy, the corneas were opened and tissues were immersed in 4 % PFA in 0.1 M PBS for 15 to 30 min fixation. For conventional electron microscopy, the fixation was carried out in 2.5 % glutaraldehyde and 3 % PFA in PBS for 2 h at room temperature, followed by incubation in 2 % OsO_4 for 2 h at 4 °C. For light microscopy, immunohistochemical labeling was performed by the indirect fluorescence method following the protocol described by Dick et al. [20].

Culture Methods

Postnatal day 3–4 (P3–P4) mouse cochleae were dissected in ice-cold PBS. The membranous labyrinth was separated from the modiolus, and the stria vascularis and spiral ligament were carefully removed. With the organ of Corti and spiral ganglion kept intact, Reissner's membrane and tectorial membrane were removed with fine forceps. The cultures were evaluated the following day using DIC optics for adhesion to the substrate. The explants were cultured in N2-supplemented DMEM with 10 % fetal bovine serum at 37°, 6.5 % CO2. In this study, the cultures can be well maintained for additional 7–10 days, and the samples were observed at P7–8. All procedures, including imaging, were performed in the culture plate with the explants remaining attached to the cover slip to facilitate preservation of the morphology of samples.

Immunohistochemistry

Cochlear tissues were fixed in 4 % PFA and dissolved in 0.1 M PBS with 30 % sucrose (pH 7.4) for 1 h at room temperature. Samples were subsequently washed three times in 0.01 M PBS and incubated for 30 min at room temperature in a blocking solution containing 5 % normal goat serum in 0.01 M PBS with 0.3 % Triton X-100. Then, the tissue was incubated at 4 °C overnight with the primary antibodies for CtbP2 (1:200, Abcam), GluR2/3 (1:100, Chemicon), Otoferlin (1:100, Abcam), MyosinVIIa (1:200, Sigma), VGLUT3 (1:150, Melipore), and NF200 (1:200, Sigma). The tissue was then washed in 0.01 M PBS three times and incubated with the secondary antibody (fluorescein isothiocyanate-conjugated goat anti-mouse IgG, 1:100, Invitrogen, CA) at room temperature for 1 h. After three additional washes, the samples were imaged directly with fluorescent microscopy to test the specificity of the primary antibody. Immunostainings without the primary antibody were also performed as a negative control (data not shown). Regions were imaged by confocal microscope (Olympus FV1000 configuration, with 1× 81 microscope, Japan). Excitation wavelengths were 488 and 647 nm, respectively. Sequence scanning was performed with an interval of 1.0 μm.

Western Blotting

Fresh cochlea from mice were obtained and prepared in 1 ml of ice-cold lysis buffer (100 mmol/L Tris/HCl, pH7.5; 100 mmol/L sodium chloride; 0.5 % deoxycholate sodium; 1 mmol/L EDTA; 1 % Nonident P40; 0.1 % sodium dodecyl sulfate, SDS, and protease inhibitor) and equal amounts of protein (50 μg each) were loaded onto 7.5 % SDS-polyacrylamide gel and electrophoretically transferred to polyvinylidene fluoride membranes (Roth, Germany). RIBEYE protein structure was detected with an anti-CtbP2 polyclonal antibody using chemiluminescence ECL substrate (Amersham, UK). AMPARs (2&3 subunits) were detected with rabbit anti-GluR2/3 (Chemicon, 1:1000). Stripped blots were re-probed with anti-β-actin polyclonal antibody (Santa Cruz, USA).

In Situ Hybridization

Antisense digoxin-labeled oligonucleotides were designed for cDNA sequence of *SMAD4* as follows: (1) 5′-ATACACCAACAAGTAATGATGCCTGTCTGA-3′; (2) 5′-TGTGGCTTCCACAAGTCAGCCTGCCAGTA-3′; (3) 5′-AAGTACTTCATACCATGCCGATTGCAGACC-3′. The standard procedure of in situ hybridization (ISH) was performed in cochlear ganglia as previously described [21].

Electron Microscopy

For scanning electron microscopy, mice were sacrificed and the cochleae were removed. All cochleae were prefixed in 2.5 % glutaraldehyde and then put in 1 % OsO_4 in 0.1 M PBS (pH 7.40) for 2 h at room temperature. After a thorough rinse in 0.1 M PBS, the specimens were then dissected in 0.1 M PBS to expose the organ of Corti. After dehydration in a graded series of alcohol, specimens were dried in an HCP-2 critical point dryer, and sputter coated with platinum for 4 min in an E-102 ion sputter. The samples were then examined by a JEOL JSM-35C scanning electron microscope (Hitachi 7100, Japan). The images were recorded digitally and photographed.

For transmission electron microscopy examination, mouse cochleae were fixed following a standard protocol [22]. For morphological analysis, the cochleae were first fixed with 4 % PFA and 2 % glutaraldehyde (pH 7.4) in PBS for 2 h and then transferred to 1 % OsO_4 at 4 °C overnight. Then they were dehydrated in graded acetone concentrations and embedded in Spurr's low viscosity epoxy resin. Semithin sections (1 μm) of

the cochlea were stained with toluidine blue for light microscopy. Ultrathin sections of the cochlea were stained with uranyl acetate and citrate and examined using a Philips CM 120 transmission electron microscope (Germany).

Whole-Cell Voltage-Clamp Recording

The whole-cell voltage-clamp techniques were used to measure nonlinear capacitance (NLC) of hair cells. The experimental chamber containing the cells was placed in the stage of an inverted microscope. The outer hair cells were bathed in the extracellular solution containing (mM) 120 NaCl, 2 $MgCl_2$, 2 $CoCl_2$, 20 TEA, 10 HEPES, and 10 4-AP. Recording pipettes, pulled from borosilicate glass with resistances between 2.5 and 4 MΩ were back-filled with solution containing (mM) 140 CsCl, 2 $MgCl_2$, 10 EGTA, and 10 HEPES. Membrane capacitance was measured using a two-sine-wave voltage stimulus protocol (10 mV peak at both 390.6 and 781.2 Hz) with subsequent fast Fourier transform-based admittance analysis from a holding potential of 0 mV. The capacitive currents were sampled at 100 kHz and low-pass filtered at 5 kHz. Series resistance was compensated off-line. Data were acquired using jClamp (Scisoft, New Haven, CT) and analyzed with Igor (WaveMetrics, Portland, OR).

The NLC can be described as the first derivative of a two-state Boltzmann function relating nonlinear charge movement to voltage. The capacitance function is described as:

$$C_m = C_{lin} + \frac{Q_{max}\alpha}{\exp\left[\alpha\left(V_m - V_{1/2}\right)\right]\left(1+\exp\left[-\alpha\left(V_m - V_{1/2}\right)\right]\right)^2}$$

where Q_{max} is maximum charge transfer in response to voltage stimulation, $V_{1/2}$ is the voltage at which the maximum charge is equally distributed across the membrane, or equivalently, the peak of the voltage-dependent capacitance. C_{lin} is linear capacitance, and $\alpha = ze/kT$ is the slope of the voltage dependence of charge transfer where k is Boltzmann's constant, T is absolute temperature, z is valence of charge movement, and e is electron charge. Data were collected from cells whose membrane resistance was greater than 500 ΩM after rupturing.

Retinal Function Test with Electroretinography

In this study, the retinal function test with electroretinography (ERG) in both wild-type (WT) and cKO mice was performed as previously described [23].

Statistical Analysis

All data are presented as mean±standard deviation. Statistical analysis for all experiments was done by one-way ANOVA with Student–Newman–Keuls test for significance ($P<0.05$), which was appropriate to determine significant differences between groups.

Results

Mice with a *SMAD4* Defect Display Auditory Neuropathy

To verify whether *SMAD4* defects contribute to auditory neuropathy, we used a mouse strain with a conditional knockout of *SMAD4* due to *SMAD4* knockout mice die in the early stages of embryogenesis. The procedure of mice generation has been described previously [9, 24], mice that were homozygous for the "floxed" *SMAD4* allele ($SMAD4^{Co/Co}$) were crossed with the Col2a1-Cre transgenic mice. In this study, we measured ABR thresholds elicited by both click and tone burst in control mice. The average hearing threshold was 48.25±5.7 dB SPL. However, no measureable ABR response was recorded for either click or tone burst in mice with a *SMAD4* defect (Fig. 1, a, b).

Next, we measured a DPOAE response to verify whether *SMAD4* defect affect the amplification of OHCs [1, 25]. DPOAE amplitudes were elicited by a pair of tone stimuli at 70 dB SPL from 6 to 30 kHz, and we found a slight reduction of DPOAE in the mice with *SMAD4* defect (Fig. 1 c), suggesting that amplification of cochlear OHCs was preserved. The value of CM, the other primary production of OHCs [1], was also examined in this study. The two curves representing CM input–output function in the mice with *SMAD4* deletion, and the controls were overall similar despite differences appearing at a few sound intensity stimulation (Fig. 1d; $p<0.05$, asterisk). These findings demonstrated that the amplification of OHCs is preserved in the mice with a *SMAD4* defect.

The *SMAD4* Defect Does Not Affect Cochlear Outer Hair Cells

We next performed a morphological and functional study of outer hair cells (OHCs) in the mice with a *SMAD4* defect. Our study showed that OHCs in $SMAD4^{-/-}$ mice were normally organized into three rows similar to the controls (Fig. 1e). Furthermore, semithin section observations showed normal localizations of OHCs in both $SMAD4^{+/+}$ and $SMAD4^{-/-}$ mice (Fig. 1f). Scanning electron microscopy (SEM) found a slight disarray of OHC stereocilia in $SMAD4^{-/-}$ mice (Fig. 1g). Transmission electron

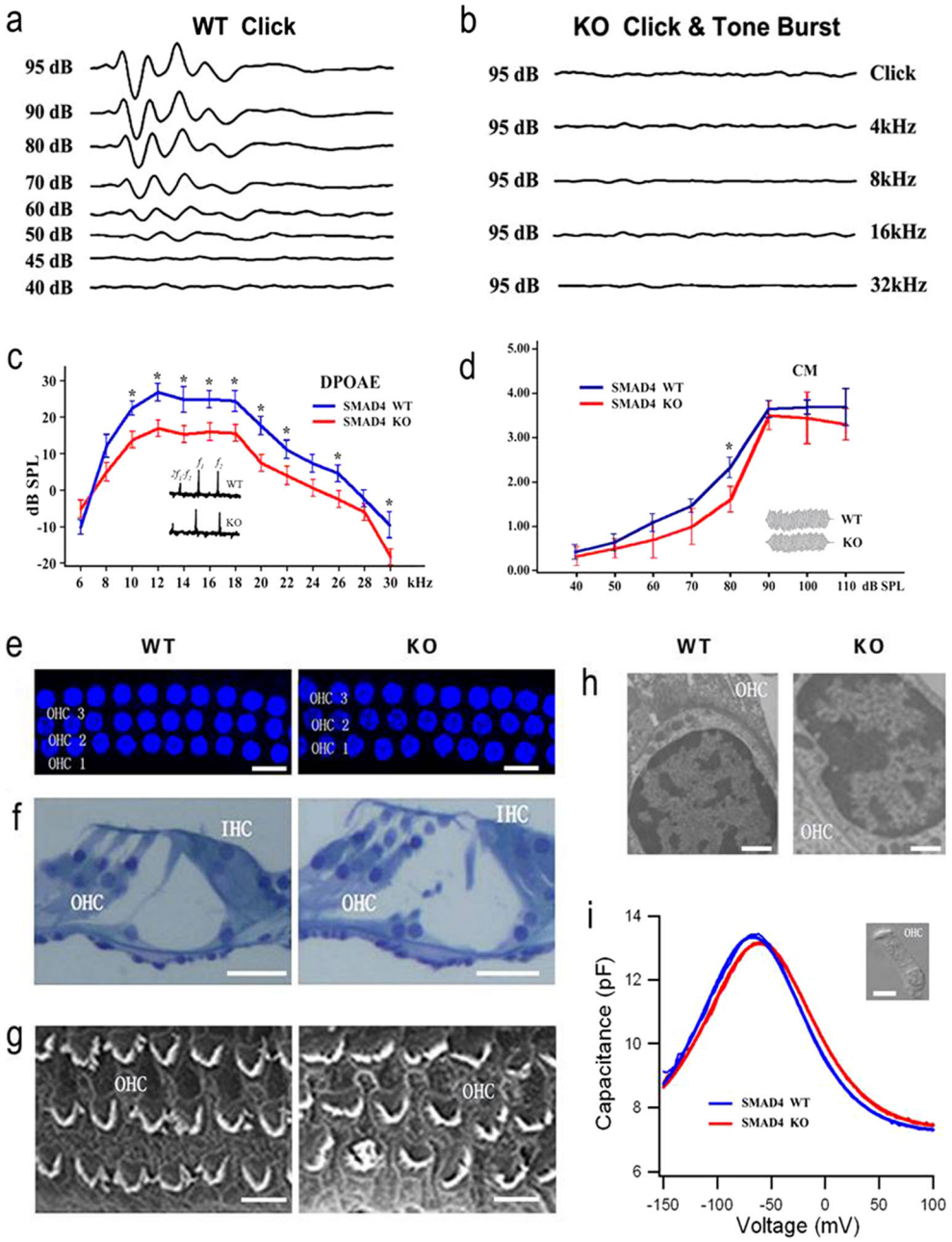

Fig. 1 Mice with a *SMAD4* defect showed features of auditory neuropathy. **a**, **b** Waveforms of ABR evoked by clicks from a $SMAD4^{+/+}$ (WT, control) and $SMAD4^{-/-}$ mice (KO). The mean ABR threshold of the control group was 48.2±5.7 dB SPL (WT, n=12). The ABRs from the $SMAD4^{-/-}$ mice were absent at 95 dB SPL (KO, n=12). The ABRs were evoked by clicks and tone burst. **c** DPOAEs were recorded from WT and KO mice (n=10), the two curves were similar overall despite reductions identified at several frequencies (in red curve, indicated by *asterisk*). The detection showed a preserved OHC function in $SMAD4^{-/-}$ mice. **d** CM detection showed nearly normal CM amplitude in both $SMAD4^{+/+}$ and $SMAD4^{-/-}$ mice (n=12). **e** Confocal microscope images revealed a normal arrangement of three rows of OHCs in $SMAD4^{-/-}$ mice (n=12). The nuclei of OHCs were labeled with DAPI staining (*blue*). *Scale bar*=5 μm. **f** The semithin sections showed a normal cochlear structure with identifiable OHCs and IHCs in $SMAD4^{-/-}$ mice (n=10). *Scale bar*=50 μm. **g** Scanning electron microscope (*SEM*) images showed a slight disarrangement of OHC stereocilia in the KO mice compared to the WT mice (n=14). *Scale bar*=5 μm. **h** Transmission electron microscope (*TEM*) images revealed a similar ultrastructure of OHCs in both $SMAD4^{+/+}$ and $SMAD4^{-/-}$ mice (n=8). *Scale bar*=2 μm. **i** NLC whole-cell patch-clamp examination showed identical curves for OHCs in both WT and KO mice (n=12). *Scale bar*=5 μm (*upper right panel*)

microscopy (TEM) showed the ultrastructures of OHCs that were unaffected in $SMAD4^{-/-}$ mice (Fig. 1h). Moreover, a possible change in electromotility of OHCs in $SMAD4^{-/-}$ mice has been examined using a whole-cell patch-clamp approach. We found an insignificant difference between mice with a *SMAD4* defect and controls (Fig. 1i). Taken

together, our study demonstrated a normal or at least preserved morphology and function of OHCs in the mice with a *SMAD4* defect.

The *SMAD4* Defect Does Not Affect Cochlear Inner Hair Cells

The inner hair cells (IHCs) of mice with *SMAD4* defect were examined using antibodies against otoferlin, VGLUT3, and myosinVIIa due to these proteins are crucial for maturation and function of afferent synapses beneath IHCs [5, 6, 26]. There were no differences observed between *SMAD4*$^{-/-}$ mice and controls (Fig. 2a–c). TEM observations also revealed unaffected stereocilia of IHCs in *SMAD4*$^{-/-}$ mice (Fig. 2d). This study suggested that *SMAD4* defect does not affect otoferlin, myosinVIIa, VGLUT3, and stereocilia in cochlear IHCs of mice.

SMAD4 Defect Causes Destruction of Cochlear Ribbon Synapses

Next, we examined whether *SMAD4* conditional knockout affected the first afferent synapse, called the ribbon synapse, which is normally formed between IHCs and spiral ganglion nerves (SGNs). The antibody identifying RIBEYE/Ctbp2, a marker for ribbon synapse, was used to label the ribbon synapse by staining both ribbons and nuclei [27]. As a result, a near absence of positive staining spots for RIBEYE/Ctbp2 was observed in the mice with *SMAD4* defect (cKO), whereas controls (WT) showed normal expression beneath IHCs (Fig. 3a, c, the left panels), suggesting that *SMAD4* defect causes disruption of cochlear ribbon synapses via damage to RIBEYE, a major pre-synaptic scaffold structure of ribbon synapses [28]. Additionally, as cochlear ribbon synapses have been characterized as glutameric [28, 29], we then examined the postsynaptic component, -amino-3-hydroxy-5-methyl-4-isoxa-zole-propionate receptor (AMPAR) by identifying the expression of GluR2/3 subunits. And we found that *SMAD4* knockout mice showed a significant reduction in GluR2/3 expression (Fig. 3a, c, the middle and right panels), suggesting that *SMAD4* defects can also significantly disrupt the postsynaptic receptors for glutamate in this synapse. Together, our study showed that *SMAD4* defect causes disruption of ribbon synapses in the cochlea of mice (Fig. 3b, d). Moreover, detection by Western blotting for both Ctbp2 and GluR2/3 showed a similar result to the examination of immunostaining (Fig. 3e, f). Further, TEM observations showed a typical ribbon synapse in control mice (Fig. 3g), whereas no distinct ribbon synapse structure can be captured in the mice with a *SMAD4* defect (Fig. 3h), confirming that *SMAD4* deficits are responsible for failed formation of cochlear ribbon synapses.

CAP is generated by electrical activity at the terminals of SGN fibers [1, 25, 30]. Therefore, CAP has been considered a functional indicator of afferent synaptic activity of the SGN fibers. In this study, we tested the CAP responses in *SMAD4*$^{-/-}$ mice. Normal CAP waveforms were observed in control mice (Fig. 3i). In contrast, no visible CAP waveforms have been identified by either click or tone burst stimuli in the mice with *SMAD4* deletions (Fig. 3j), supporting that *SMAD4* defect induces a functional collapse of cochlear ribbon synapses.

Ribbon Synapse Does Not Develop at Basilar Membrane of *SMAD4*$^{-/-}$ Mice In Vitro

To examine whether the failed formation of cochlear ribbon synapse has been caused by abnormal secretion of cartilage tissue, the basilar membranes from *SMAD4*$^{-/-}$ mice were harvested to culture. In this study, the samples were collected at P3–4 and strong signals of Ctbp2 (green) and GluR2/3 (red) were found at p6–7 blew the IHCs of WT sample. However, there were no any positive signals of both Ctbp2 and GluR2/3 can be found at the samples from cKO mice (Fig. 4). Our study

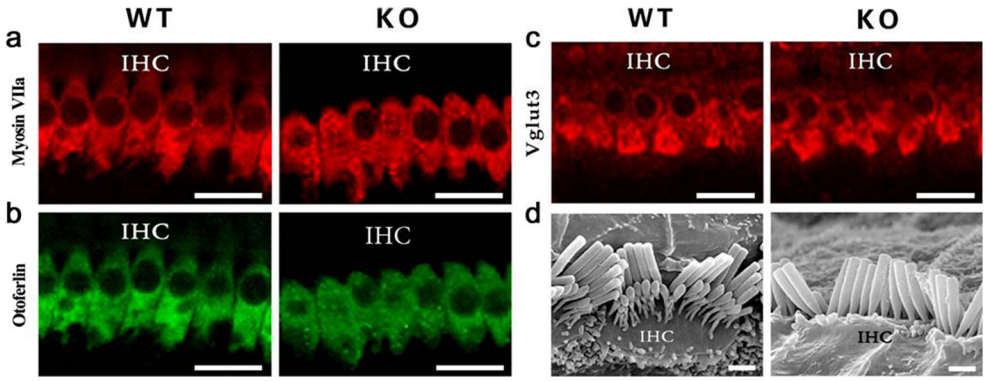

Fig. 2 *SMAD4* defect does not affect the morphology of inner hair cells. Three important proteins in IHCs (MyosinVIIa, Otoferlin, and VGLUT3) were tested. **a**–**c** MyosinVIIa (**a**, *red*), Otoferlin (**b**, *green*), and VGLUT3 (**c**, *red*) showed normal patterns of expression in both adult *SMAD4*$^{+/+}$ and *SMAD4*$^{-/-}$ mice (WT, n=10; KO, n=10). *Scale bar*=10 μm. **d** SEM images showed normal stereocilia in IHCs for both WT and KO mice (WT, n=14; KO, n=14). *Scale bar*=10 μm

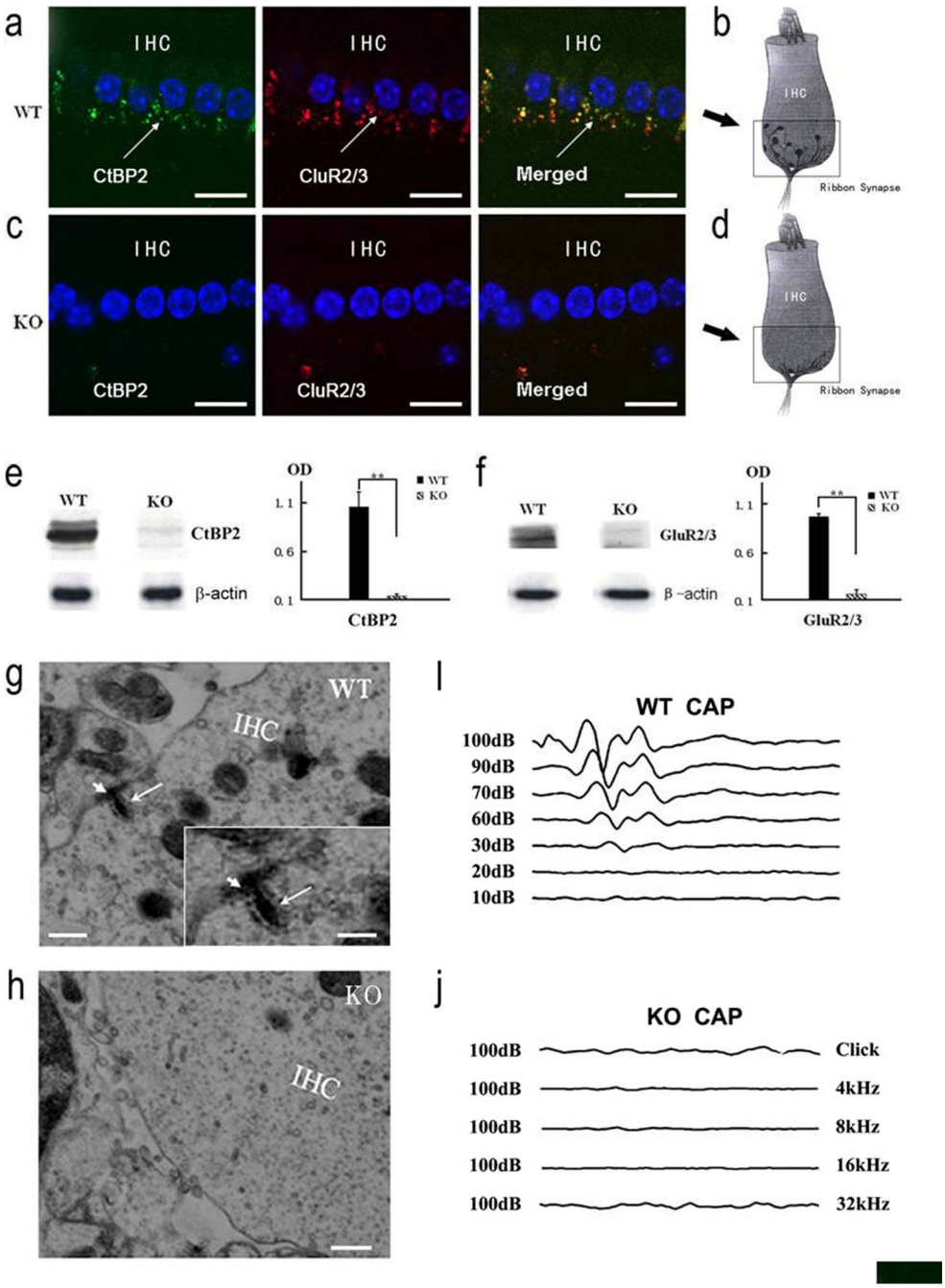

Fig. 3 *SMAD4* defect causes destruction of cochlear ribbon synapse. **a** The immunostaining detections showed normal staining signals of RIBEYE/CtBP2 beneath IHCs in adult WT mice (*green*, *left panel*); The normal signals of GluR2/3 were also visualized (*red*, *middle panel*); The merged signals showed an intact ribbon synapses (*orange*, *right panel*). **b** The schematic of **a. c** No obvious positive signals of RIBEYE/CtBP2 or GluR2/3 have been found in the cKo mice. **d** The schematic of **c**. *Scale bar*=10 μm (**a**, **b**). **e**, **f** Western blot analysis showed an extremely low level of RIBEYE/CtBP2 and GluR2/3 in the cochlea of cKo mice compared to the controls ($p<0.01$, *double asterisk*). **g** A typical ribbon synapse was observed by TEM study in the cKo mice ($n=6$). The synaptic vesicles were in the ring-shape tethered to the ribbon (*long arrow*). The *short arrow* indicates postsynaptic density. *Scale bar*=100 nm. The *lower right frame* is the enlarged image of the ribbon synapse above. *Scale bar*=50 nm. **h** No identifiable ribbon synapses were observed in cKo mice ($n=12$). *Scale bar*=100 nm. **i** The CAP waveforms recorded from the WT mice before TEM detection, the mean CAP threshold of the WT mice was 27.1±3.6 dB SPL ($n=12$). **j** The CAP waveforms of cKo mice were absent before the TEM observations (clicks and tone burst, $n=6$)

confirms that *SMAD4* deficits can cause a failure of ribbon synapse formation and suggests that the failed development of cochlear ribbon synapse has not been associated with additional factors, such as abnormal secretion of cartilage tissue.

Reduction of *SMAD4* Transcription in Auditory Nerves Causes Failed Development of Cochlear Ribbon Synapses

To verify whether disruption of ribbon synapses is responsible for the auditory neuropathy observed in $SMAD4^{-/-}$ mice, we next examined the developmental profiles of cochlear ribbon synapses. It has been reported that exogenous expression of RIBEYE in transfected R28 cells can lead to protein aggregates which were often surrounded by vesicles, indicating that RIBEYE alone can establish ribbon-like structures [31, 32]. Here, our study showed nearly no positive signals for RIBEYE/Ctbp2 at the postnatal 0, 7, or 14 day (P0, P7, or P14) in $SMAD4^{-/-}$ mice (Fig. 5a–c, lower panels), suggesting that cochlear ribbon synapses have not developed in $SMAD4^{-/-}$ mice. In contrast, positive signals have been clearly identified at P7 in the basal

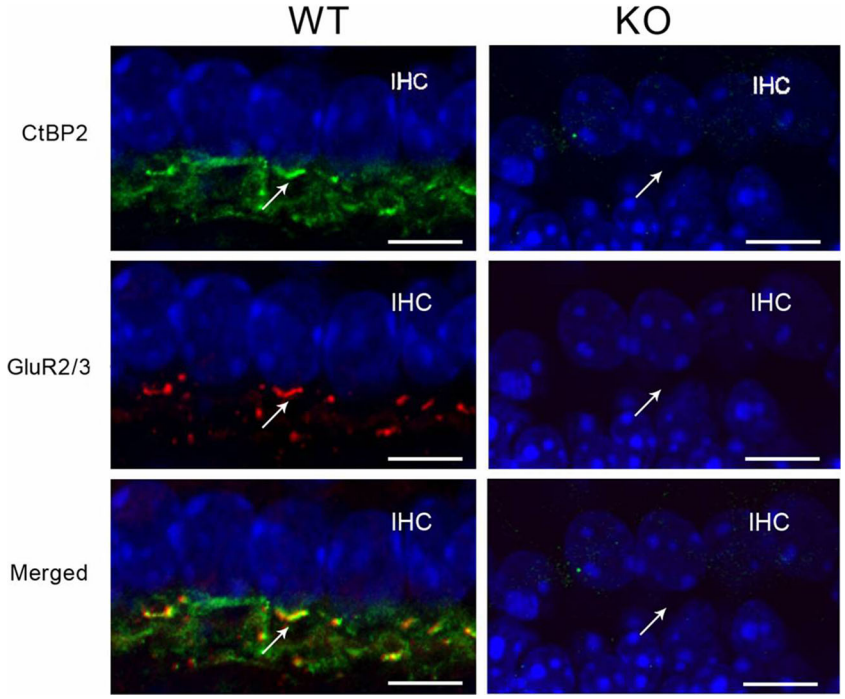

Fig. 4 Cochlear ribbon synapses are unable to develop in vitro. Organotypic cochlear explants included the organ of Corti and associated spiral ganglion, were collected at P3–4, and cultured for additional 3–4 days. Nuclei of hair cells are labeled with DAPI (*blue*). Presynaptic ribbons in the IHCs were labeled by anti-CtbP2 (*green*), which are on the basolateral region of the IHCs. Post synapse receptors (AMPARs) were labeled by anti-GluR2/3 (*red*), which are on the SGN peripheral processes apposed to the basolateral region of the IHCs. Co-localization of presynaptic ribbons (positive CtpP2 signals, *red*, shown in the *upper left panel*), and postsynaptic receptors (positive GluR2/3 signals, *green*, shown in *middle left panel*) were identified closed to IHCs in the culture samples of WT mice (positive merged signals, *orange*, shown in *lower left panel*). In contrast, there was either positive CtpP2 or GluR2/3 signals that can be identified in the culture samples of cKO mice. *Scale bar*=2 μm

turn of cochlear basal membranes in control mice (Fig. 5b, upper right panel). Further, multiple positive spots appear at the apical, middle, and basal turns in control mice at P14 (Fig. 5c, upper panels). Therefore, our study confirmed that *SMAD4* defects could affect the formation of cochlear ribbon synapses, leading to a subsequent auditory neuropathy.

To determine how *SMAD4* deletion causes failed formation of cochlear ribbon synapses, we detected changes in *SMAD4* messenger RNA (mRNA) levels in auditory nerves using an in situ hybridization approach. Auditory nerves are crucial in targeting the pre-synaptic components (IHCs) to build ribbon synaptic structures [33]. Our study showed a high level of *SMAD4* mRNA in auditory nerves at P7 and P14 in controls (Fig. 5d)—a critical period of formation for cochlear ribbon synapses [33]. In contrast, a dramatic reduction in *SMAD4* mRNA was identified at P7 and P14 in mice with *SMAD4* defect (Fig. 5e), suggesting that reduced transcription of *SMAD4* could contribute to the disruption of synapses and consequent hearing disorder. As we observed a lack of recording of ABRs at P14 in $SMAD4^{-/-}$ mice compared with controls (Fig. 5f), this evidence supports the hypothesis that a *SMAD4* deficit causes functional reduction in hearing.

Hearing Loss in $SMAD4^{-/-}$ Mice Were Restored by an Electrical Stimulation Toward Auditory Nerves

Importantly, we recorded a distinct eEBR waveform using an artificial electrical stimulation toward the auditory nerves in $SMAD^{-/-}$ mice (Fig. 6a), suggesting that deafness (auditory neuropathy) can be restored in a mice with a *SMAD4* defect. In addition, this evidence confirmed that disruption of ribbon synapse in the cochlea is primary site of lesion responsible for AN. To test why eEBR response can be evoked in mice with *SMAD4* defect, we detected a morphological manifestation of the postsynaptic auditory nerve in $SMAD4^{-/-}$ mice. We found a normal density of spiral ganglion cells (SGCs) and approximate neuronal innervations in both $SMAD4^{-/-}$ and control mice (Fig. 6b), supporting functional recovery of hearing in $SMAD4^{-/-}$ mice. Further, the evidence also showed that the *SMAD4* defect does not significantly affect the postsynaptic auditory nerves.

SMAD4 Defect Does Not Affect the Retinal Ribbon Synapses and Visional Function

Besides the inner ear in mammals, ribbon synapses have also been found in the retina [27, 34]. As such, we wanted to know whether *SMAD4* is critical for retinal ribbon synapses. We

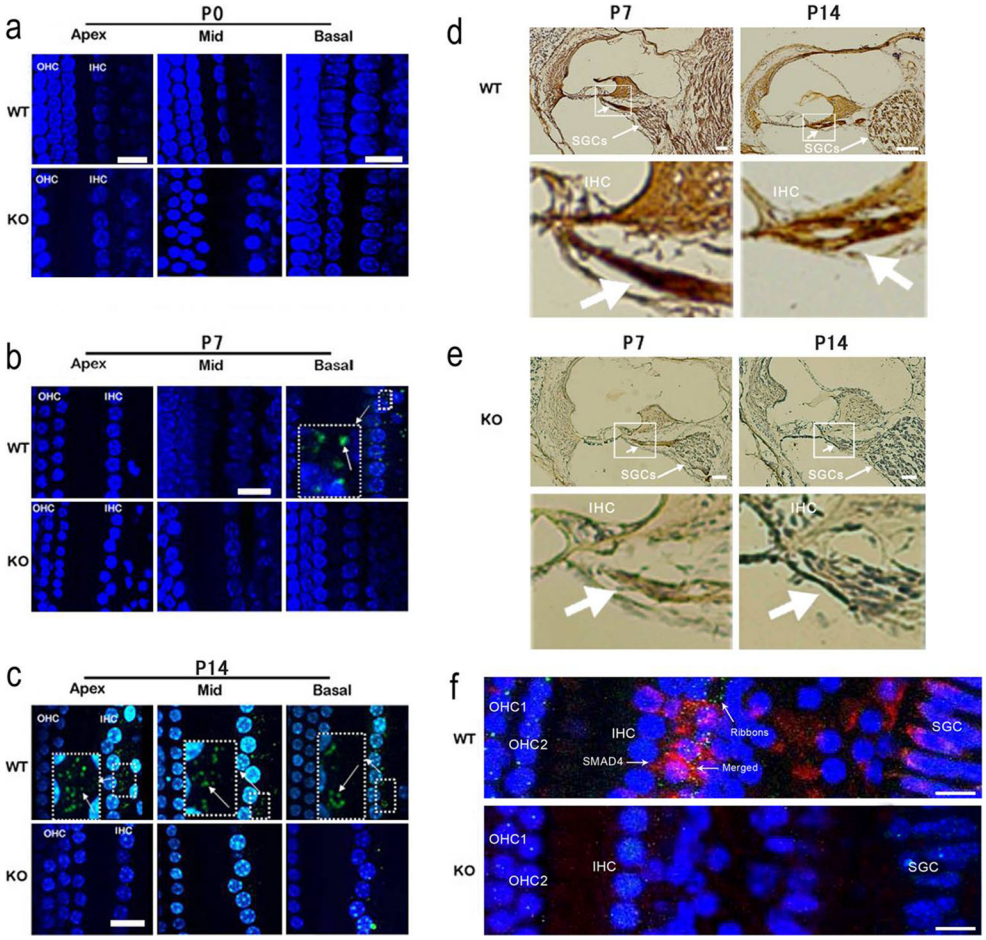

Fig. 5 Reduction of *SMAD4* expression in auditory nerves is responsible for the failed development of ribbon synapses. RIBEYE/Ctbp2 immunostaining was used to label the cochlear ribbon synapses in this study. **a** There were no positive spots at P0 from either the KO or WT mice (n=12). *Scale bar*=10 μm (except *upper right panel* where the scale=15 μm). The nuclei were stained with DAPI (*blue*). **b** Ctbp2-positive signals were identified in the basal turn of WT mice at P7. The *enlarged frame with dashed line* shows positive spots labeling the ribbons (*green*, *upper right panel*). No identifiable spots of Ctbp2 were observed in KO mice at P7 (the *lower panel*, n=12). *Scale bar*=10 μm (except *upper middle panel* where the scale=5 μm). **c** Abundant Ctbp2 immunostaining spots were identified beneath the IHCs of WT mice at P14 (*upper panel*, anti-Ctbp2 also showed strong nuclei staining), whereas no identifiable spots of Ctbp2 were observed in KO mice at P14 (*lower panel*, n=16). *Scale bar*=10 μm. **d** WT mice at P7 and P14 showed a strong expression of *SMAD4* mRNA in both postsynaptic spiral ganglion cells (*SGCs*, *upper panels*, *short arrows*) and nerves (*SGNs*, *upper panels*, *long arrows*). *Lower panels* are enlarged images of the *framed areas of the upper panels*. **e** KO mice showed a dramatic reduction of *SMAD4* mRNA in SGCs (*upper panels*, *short arrows*) and nerves (*SGNs*, *upper panels*, *long arrows*) at P7 and P14. The *lower panels* are enlarged images of the *framed areas of the upper panels*. *Scale bar*=50 μm. **f** WT mice at P14 showed a normal ABR response (*upper panel*), whereas no ABR response was observed at P14 in KO mice (*lower panel*)

tested RIBEYE/Ctbp2 expression in the outer plexiform layer (OPL) in a $SMAD4^{-/-}$ and a control mouse. No significant differences in RIBEYE/Ctbp2 expression were found between $SMAD4^{-/-}$ and control mice (Fig. 7a–g), suggesting that the *SMAD4* defect does not affect the retinal ribbon synapses. The finding was further confirmed by Western blot analysis of RIBEYE/Ctbp2 detection; there was no difference between $SMAD4^{-/-}$ and control mice (Fig. 7h, i, p>0.05). Moreover, the visual function of $SMAD4^{-/-}$ mice was also tested. Our study revealed that there were identical electroretinography (ERG) responses in both $SMAD4^{-/-}$ and control mice, suggesting that the *SMAD4* defect does not affect the retinal ribbon synapses and visual function (Fig. 7j, k).

Discussion

This study demonstrated for the first time that may cause auditory neuropathy by significantly disrupting cochlear ribbon synapses. This notion has been further supported by the restoration of hearing after electrical stimuli were employed toward post-synaptic auditory nerves in $SMAD4^{-/-}$ mice. Moreover, our study demonstrated that *SMAD4* defect does not affect the ribbon synapses of retina, as well as visional ability.

Until now, *SMADs* were normally described as critical inhibitory genes in the TGF-β and BMP-4 signaling pathway [35, 36]. Additionally, BMP4 has been reported to promote

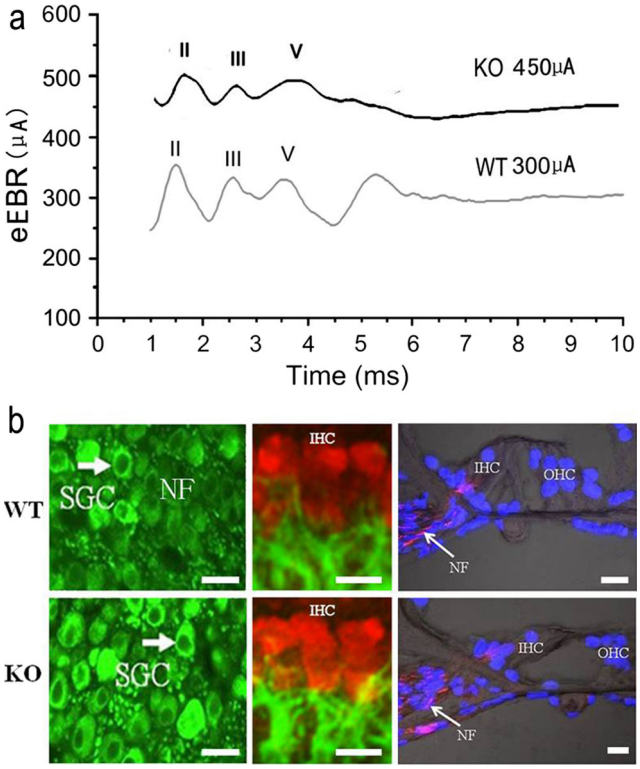

Fig. 6 Restoration of hearing disorder in cKo mice has been achieved by the electrical stimulations toward auditory nerves. **a** A reduced but distinct eEBR was evoked in *SMAD4*$^{-/-}$ mice by an electrical stimulation using a fine electrode compared with *SMAD4*$^{+/+}$ mice. Stimulated intensities were 300 μA (WT) and 450 μA (KO), respectively. **b** There was an identical density of SGCs in both *SMAD4*$^{+/+}$ and *SMAD4*$^{-/-}$ mice (*green*, *left panel*); normal connections of auditory nerves (*green*) contacting IHCs (*red*, labeled by anti-myosinVIIa) were observed in both *SMAD4*$^{+/+}$ and *SMAD4*$^{-/-}$ mice (*middle panel*); auditory nerves from both WT and KO mice showed a normal innervations to hair cells (*red*, labeled by anti-NF200, *right panel*); *bar*=5 μm

differentiation and reinnervation of sensory neurons from human embryonic stem cells [16]. Although our previous studies revealed that *SMAD4* deletion induces a disorder of hearing and balance [9, 37], it remained unclear how *SMAD4* defects cause deafness. Here, we reported that *SMAD4* defects can induce failed development of cochlear ribbon synapses. To our knowledge, these findings are the initial evidence supporting *SMAD4* as essential for the formation of cochlear ribbon synapses.

SMAD4 is Essential for the Formation of Cochlear Ribbon Synapses

Ribbon synapses tend to alter in response to multiple stimulations, reflecting a structural and functional adaptation of synaptic plasticity in the cochlea [38]. RIBEYE, a specific scaffolding protein, constitutes a major pre-synaptic component of the ribbon synapse and contributes an important role in the formation and organization of this synapse [27, 31, 39]. Lack of RIBEYE can inhibit late steps in the development of bipolar cells and induces apoptosis [39]. Knockdown of RIBEYE expression impairs hearing and visual function [39, 40]. Here, our study demonstrated that *SMAD4* defects cause a significant reduction of RIBEYE at cochlear ribbon synapses, which may result in structural destruction and functional loss of the synapse. Besides the lack of RIBEYE, our study also showed an extremely low level of GluR2&3 expression in *SMAD4*$^{-/-}$ mice, indicating that RIBEYE deficiency could cause a secondary loss of postsynaptic AMPA receptors. As AMPA receptors have been proposed to be responsible for the generation of excitatory responses in the cochlea [22, 30, 41], this finding provides evidence that *SMAD4* defects disrupt the generation of glutamatergic excitability in the cochlea.

SMAD4 Defect Exclusively Disrupt the Ribbon Synapses in the Cochlea

Ribbon synapses have been fully reported to develop in both the cochlea and retina in mammals [5, 28, 29]. However, the distinctions between the ribbon synapses located in the ear and eye have not been well characterized so far [29, 34]. Here, our study showed that *SMAD4* deficits exclusively interrupt the development of ribbon synapses in the inner ear, but not the formation of ribbon synapses in the retina in mice. Our study therefore indicates a different mechanism of ribbon synapse construction between the cochlea and retina, which *SMAD4* participation may lead to the distinctions.

The *SMAD4* Gene Is Associated with Auditory Neuropathy

In this study, the deafness associated with *SMAD4* defects has been characterized by recorded potentials in auditory nerves and brainstem, coupled with preserved function of cochlear amplification. This type of deafness indicates auditory neuropathy and a defect in cochlear ribbon synapses [1, 3], suggesting a connection between *SMAD4* and auditory neuropathy.

Several lines of evidence in this study support the notion that *SMAD4* deficits are responsible for auditory neuropathy: (1) The mice with *SMAD4* defect mimicked auditory neuropathy by displaying an absence of ABR responses, with preserved or normal DPOAE and CM responses. (2) *SMAD4* defect in mice led to failed formation of cochlear ribbon synapses, near the junction of IHCs and SGNs. (3) *SMAD4* deficits caused a dramatic reduction in transcription in the auditory nerve during the critical duration of ribbon synapse development. The terminals of the auditory nerve are crucial in targeting pre-synaptic inner hair cells (IHCs) during the period of ribbon synaptic construction. Thus, a lack of SMAD4 in the postsynaptic auditory nerves disturbs ribbon synapse formation. (4) Deafness in *SMAD4* knockout

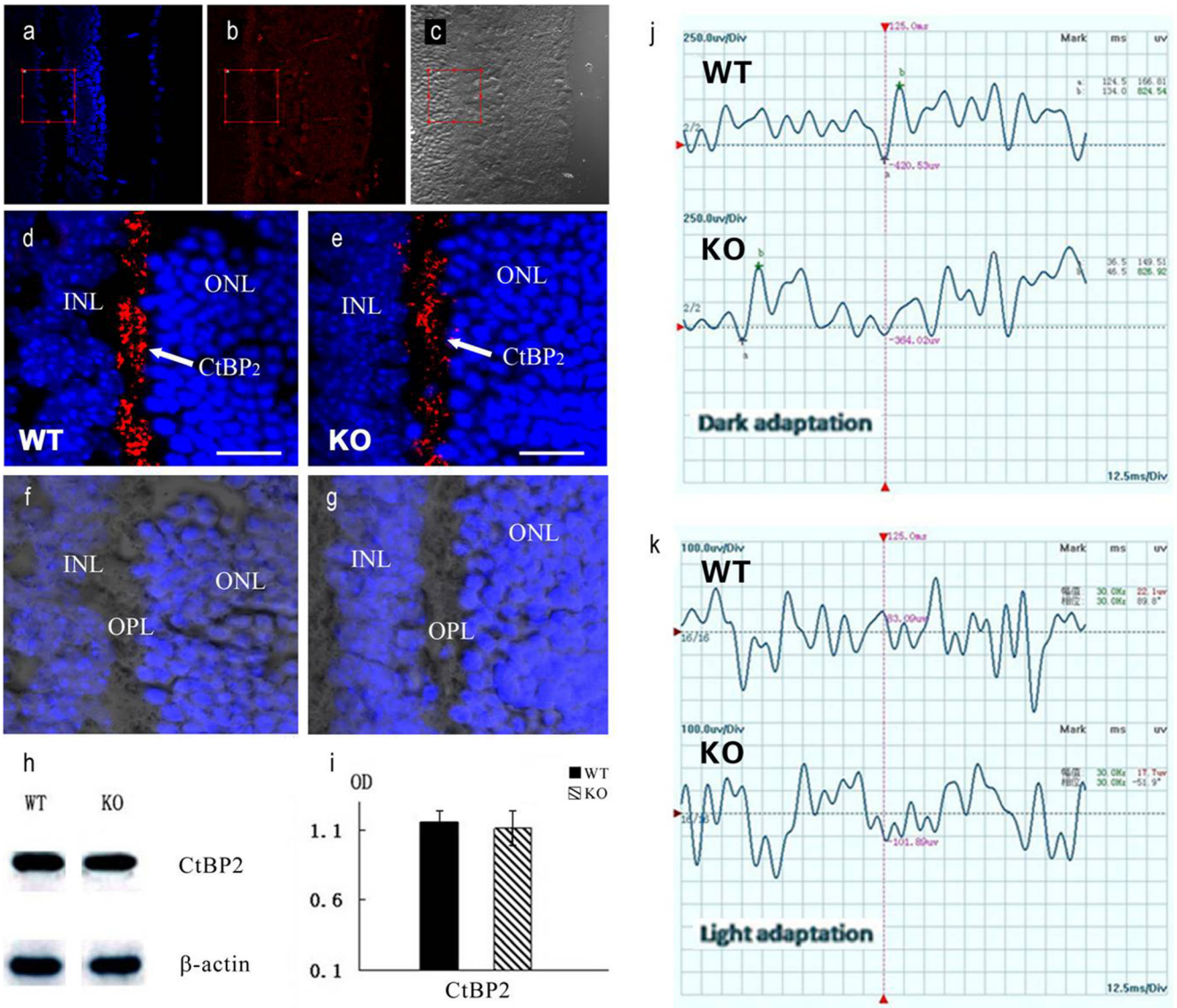

Fig. 7 *SMAD4* defect does not disturb retinal ribbon synapses and visual function in mice. **a**–**c** Confocal images under the conditions of DAPI staining (*blue*), anti-RIBEYE/Ctbp2 immunostaining (*red*), and the differential interference contrast (*DIC*), respectively. The *red frames* of indicate outer plexiform layers (*OPL*) in a vertical cryostat section through the retina of mice. **d**, **e** RIBEYE/Ctbp2 staining from the retina of a $SMAD4^{+/+}$ mouse (*left*) and a $SMAD4^{-/-}$ mouse (*right*). Similar photoreceptor ribbon synapses labeled by anti-RIBEYE/Ctbp2 are found in the OPL in the retina of $SMAD4^{+/+}$ mice (*arrow*, WT, $n=10$) and $SMAD4^{-/-}$ mice (*arrow*, KO, $n=16$). **f**, **g** The DIC images of the retina of a $SMAD4^{+/+}$ mouse (**d**) and a $SMAD4^{-/-}$ mouse (**e**), respectively. **d**–**g** *Scale bar*=20 μm. **h**, **i** Quantitative analysis of Western blotting showed no significant difference in retinal RIBEYE/Ctbp2 expression between $SMAD4^{+/+}$ and $SMAD4^{-/-}$ mice ($p>0.05$). **j**, **k** There are normal ERG responses in both $SMAD4^{+/+}$ and $SMAD4^{-/-}$ mice detected by dark and light adaptations (WT, $n=10$; KO, $n=10$). *INL* inner nucleus layer, *ONL* outer nucleus layer

mice has been restored by electrical stimulation. Of note, our study showed a reduced eABR value that the hearing restoration is incomplete in $SMAD4^{-/-}$ mice. A possible explanation is that the $SMAD4^{-/-}$ mice were chosen at the age of 8 weeks to avoid the high possibility of death which caused by a surgical procedure to record eABR. A long duration of lacking sound stimulation can lead to significant degeneration of auditory nerves; thus, considerable degenerations of auditory nerves may cause a reduced response to electrical stimuli, although our study demonstrated that *SMAD4* deficits do not disrupt the post-synaptic auditory nerve.

A number of genes have been proposed to associate with auditory neuropathy. For instance, mice lacking otoferlin or VGLUT3 are profoundly deaf, with no detectable ABR across all sound frequencies. DPOAE examinations revealed normal cochlear amplification [29]. More than 50 % of subjects carrying biallelic *otof* mutations show preserved function of OHCs [42]. Further study found that mice with *otof* deletions display an impaired synchronous synaptic transmission which

was unable to evoke normal glutamate release at cochlear ribbon synapses [5]. Our study demonstrated that *SMAD4* is required for cochlear ribbon synapse formation. In contrast, *OTOF* is not essential for ribbon synaptic formation but is essential for the exocytosis of cochlear ribbon synapses [5]. Mice lacking VGLUT3 showed elongated ribbon shape. *VGLUT3*$^{-/-}$ mice are profoundly deaf due to the absence of glutamate release from IHCs [30]. Supporting results were obtained from DFNB9 patients: a defect of synchronous IHC synaptic transmission underlies the mechanism of auditory neuropathy and could explain poor speech discrimination [5, 27]. *DIAPH3* has been reported to be involved in non syndromic auditory neuropathy. *DIAPH3* mutation causes overexpression of the DIAPH3 protein and impairs hair cell function [7]. Together, an emerging possibility is that these deafness-associated genes could be classified as a neurological entity referred to as IHCs synaptopathy.

Previous studies by Caputo and Le Goff reported that several heterozygous missense *SMAD4* mutations in subjects with Myhre syndrome [10, 11]. Sensorineural deafness is one of the major features of this rare syndrome, supporting a connection between *SMAD4* deficits and hearing loss. However, it is unclear whether a lesion of cochlear ribbon synapses is responsible the deafness of Myhre syndrome. Anyhow, given the benefit of cochlear implants to DFNB9 patients, a deafness caused by the defect of ribbon synapse [5], our findings therefore may indicate a therapeutic prospect to address deafness and poor speech perception associated with *SMAD4* defects, which could potentially be restored by cochlear implant.

Acknowledgments This work was supported by grants from the National Basic Research Program of China (973Program) (2012CB967900; 2012CB967901) and Beijing Natural Science Foundation (5122040). Additionally, this work was supported by grants from the China Postdoctoral Science Foundation (201003779; 20100470103) and the National Natural Science Foundation of China (NSFC) (31040038).

Compliance with Ethical Standards All procedures were executed in accordance with an animal protocol approved by the Animal Care and Use Committee of the Institute of Biotechnology of AMMS and the Institute of Otolaryngology, the General Hospital of Chinese PLA.

Conflict of Interest The authors declare that they have no competing interests.

References

1. Starr A, Picton TW, Sininger Y, Hood LJ, Berlin CI (1996) Auditory neuropathy. Brain 119(Pt 3):741–753
2. Berlin CI, Hood LJ, Morlet T, Wilensky D, Li L, Mattingly KR, Taylor-Jeanfreau J, Keats BJ et al (2010) Multi-site diagnosis and management of 260 patients with auditory neuropathy/dys-synchrony (auditory neuropathy spectrum disorder). Int J Audiol 49(1):30–43
3. Moser T, Predoehl F, Starr A (2013) Review of hair cell synapse defects in sensorineural hearing impairment. Otol Neurotol 34(6): 995–1004
4. Varga R, Kelley PM, Keats BJ, Starr A, Leal SM, Cohn E, Kimberling WJ (2003) Non-syndromic recessive auditory neuropathy is the result of mutations in the otoferlin (OTOF) gene. J Med Genet 40(1):45–50
5. Roux I, Safieddine S, Nouvian R, Grati M, Simmler MC, Bahloul A, Perfettini I, Le Gall M et al (2006) Otoferlin, defective in a human deafness form, is essential for exocytosis at the auditory ribbon synapse. Cell 127(2):277–289
6. Ruel J, Emery S, Nouvian R, Bersot T, Amilhon B, Van Rybroek JM, Rebillard G, Lenoir M et al (2008) Impairment of SLC17A8 encoding vesicular glutamate transporter-3, VGLUT3, underlies nonsyndromic deafness DFNA25 and inner hair cell dysfunction in null mice. Am J Hum Genet 83(2):278–292
7. Schoen CJ, Emery SB, Thorne MC, Ammana HR, Sliwerska E, Arnett J, Hortsch M, Hannan F et al (2010) Increased activity of diaphanous homolog 3 (DIAPH3)/diaphanous causes hearing defects in humans with auditory neuropathy and in Drosophila. Proc Natl Acad Sci U S A 107(30):13396–13401
8. Yasunaga S, Grati M, Cohen-Salmon M, El-Amraoui A, Mustapha M, Salem N, El-Zir E, Loiselet J et al (1999) A mutation in OTOF, encoding otoferlin, a FER-1-like protein, causes DFNB9, a nonsyndromic form of deafness. Nat Genet 21(4):363–369
9. Yang SM, Hou ZH, Yang G, Zhang JS, Hu YY, Sun JH, Guo WW, He D et al (2009) Chondrocyte-specific Smad4 gene conditional knockout results in hearing loss and inner ear malformation in mice. Dep Dyn 238(8):1897–1908
10. Caputo V, Cianetti L, Niceta M, Carta C, Ciolfi A, Bocchinfuso G, Carrani E, Dentici ML et al (2012) A restricted spectrum of mutations in the SMAD4 tumor-suppressor gene underlies Myhre syndrome. Am J Hum Genet 90(1):161–169
11. Le Goff C, Mahaut C, Abhyankar A, Le Goff W, Serre V, Afenjar A, Destree A, di Rocco M et al (2012) Mutations at a single codon in Mad homology 2 domain of SMAD4 cause Myhre syndrome. Nat Genet 44(1):85–88
12. Jones CM, Lyons KM, Hogan BL (1991) Involvement of bone morphogenetic protein-4 (BMP-4) and Vgr-1 in morphogenesis and neurogenesis in the mouse. Development 111(2):531–542
13. Nakayama N, Lee J, Chiu L (2000) Vascular endothelial growth factor synergistically enhances bone morphogenetic protein-4-dependent lymphohematopoietic cell generation from embryonic stem cells in vitro. Blood 95(7):2275–2283
14. Nakayama T, Cui Y, Christian JL (2000) Regulation of BMP/Dpp signaling during embryonic development. Cell Mol Life Sci 57(6): 943–956
15. Wijgerde M, Karp S, McMahon J, McMahon AP (2005) Noggin antagonism of BMP4 signaling controls development of the axial skeleton in the mouse. Dev Biol 286(1):149–157
16. Shi F, Corrales CE, Liberman MC, Edge AS (2007) BMP4 induction of sensory neurons from human embryonic stem cells and reinnervation of sensory epithelium. Eur J Neurosci 26(11):3016–3023
17. Yang X, Li C, Herrera PL, Deng CX (2002) Generation of Smad4/Dpc4 conditional knockout mice. Genesis 32(2):80–81
18. Le Calvez S, Avan P, Gilain L, Romand R (1998) CD1 hearing-impaired mice. I: distortion product otoacoustic emission levels, cochlear function and morphology. Hear Res 120(1–2):37–50
19. Dick O, Hack I, Altrock WD, Garner CC, Gundelfinger ED, Brandstatter JH (2001) Localization of the presynaptic cytomatrix protein Piccolo at ribbon and conventional synapses in the rat retina: comparison with Bassoon. J Com Neurol 439(2):224–234
20. Dick O, tom Dieck S, Altrock WD, Ammermuller J, Weiler R, Garner CC, Gundelfinger ED, Brandstatter JH (2003) The

presynaptic active zone protein bassoon is essential for photoreceptor ribbon synapse formation in the retina. Neuron 37(5):775–786
21. Niedzielski AS, Wenthold RJ (1995) Expression of AMPA, kainate, and NMDA receptor subunits in cochlear and vestibular ganglia. J Neurosci 15(3 Pt 2):2338–2353
22. Matsubara A, Laake JH, Davanger S, Usami S, Ottersen OP (1996) Organization of AMPA receptor subunits at a glutamate synapse: a quantitative immunogold analysis of hair cell synapses in the rat organ of Corti. J Neurosci 16(14):4457–4467
23. Ciavatta VT, Kim M, Wong P, Nickerson JM, Shuler RK Jr, McLean GY, Pardue MT (2009) Retinal expression of Fgf2 in RCS rats with subretinal microphotodiode array. Invest Ophthalmol Vis Sci 50(10):4523–4530
24. Zhou YX, Zhao M, Li D, Shimazu K, Sakata K, Deng CX, Lu B (2003) Cerebellar deficits and hyperactivity in mice lacking Smad4. J Biol Chem 278(43):42313–42320
25. Ohashi T, Ochi K, Nishino H, Kenmochi M, Yoshida K (2005) Recovery of human compound action potential using a paired-click stimulation paradigm. Hear Res 203(1–2):192–200
26. Heidrych P, Zimmermann U, Kuhn S, Franz C, Engel J, Duncker SV, Hirt B, Pusch CM et al (2009) Otoferlin interacts with myosin VI: implications for maintenance of the basolateral synaptic structure of the inner hair cell. Hum Mol Genet 18(15):2779–2790
27. Khimich D, Nouvian R, Pujol R, tom Dieck S, Egner A, Gundelfinger ED, Moser T (2005) Hair cell synaptic ribbons are essential for synchronous auditory signalling. Nature 434(7035): 889–894
28. Moser T, Brandt A, Lysakowski A (2006) Hair cell ribbon synapses. Cell Tissue Res 326(2):347–359
29. Gomez-Casati ME, Murtie JC, Rio C, Stankovic K, Liberman MC, Corfas G (2010) Nonneuronal cells regulate synapse formation in the vestibular sensory epithelium via erbB-dependent BDNF expression. Proc Natl Acad Sci U S A 107(39):17005–17010
30. Seal RP, Akil O, Yi E, Weber CM, Grant L, Yoo J, Clause A, Kandler K et al (2008) Sensorineural deafness and seizures in mice lacking vesicular glutamate transporter 3. Neuron 57(2):263–275
31. Magupalli VG, Schwarz K, Alpadi K, Natarajan S, Seigel GM, Schmitz F (2008) Multiple RIBEYE-RIBEYE interactions create a dynamic scaffold for the formation of synaptic ribbons. J Neurosci 28(32):7954–7967
32. Sheets L, Trapani JG, Mo W, Obholzer N, Nicolson T (2011) Ribeye is required for presynaptic Ca(V)1.3a channel localization and afferent innervation of sensory hair cells. Development 138(7): 1309–1319
33. Wang Q, Green SH (2011) Functional role of neurotrophin-3 in synapse regeneration by spiral ganglion neurons on inner hair cells after excitotoxic trauma in vitro. J Neurosci 31(21):7938–7949
34. Zanazzi G, Matthews G (2009) The molecular architecture of ribbon presynaptic terminals. Mol Neurobiol 39(2):130–148
35. Gerlach LM, Hutson MR, Germiller JA, Nguyen-Luu D, Victor JC, Barald KF (2000) Addition of the BMP4 antagonist, noggin, disrupts avian inner ear development. Development 127(1):45–54
36. Thompson DL, Gerlach-Bank LM, Barald KF, Koenig RJ (2003) Retinoic acid repression of bone morphogenetic protein 4 in inner ear development. Mol Cell Biol 23(7):2277–2286
37. Yang SM, Deng AC, Huang DL, Sun JH, Yang G, Yu YP, Hou ZH, Guo WW et al (2011) The role of Smad4 in vestibular development in mice. Int J Dev Neurosci 29(1):15–23
38. Wang Y, Manis PB (2005) Synaptic transmission at the cochlear nucleus endbulb synapse during age-related hearing loss in mice. J Neurophysiol 94(3):1814–1824
39. Wan L, Almers W, Chen W (2005) Two ribeye genes in teleosts: the role of Ribeye in ribbon formation and bipolar cell development. J Neurosci 25(4):941–949
40. Brockerhoff SE, Hurley JB, Janssen-Bienhold U, Neuhauss SC, Driever W, Dowling JE (1995) A behavioral screen for isolating zebrafish mutants with visual system defects. Proc Natl Acad Sci U S A 92(23):10545–10549
41. tom Dieck S, Sanmarti-Vila L, Langnaese K, Richter K, Kindler S, Soyke A, Wex H, Smalla KH et al (1998) Bassoon, a novel zinc-finger CAG/glutamine-repeat protein selectively localized at the active zone of presynaptic nerve terminals. J Cell Biol 142(2): 499–509
42. Rodriguez-Ballesteros M, Reynoso R, Olarte M, Villamar M, Morera C, Santarelli R, Arslan E, Meda C et al (2008) A multicenter study on the prevalence and spectrum of mutations in the otoferlin gene (OTOF) in subjects with nonsyndromic hearing impairment and auditory neuropathy. Hum Mutat 29(6):823–831